Journal of Sound and Vibration (1997) **204**(4), 561–574

AN APPROXIMATION TO THE VIBRATIONS OF OBLATE SPHEROIDAL SHELLS

A. M. Al-Jumaily† and F. M. Najim

Mechanical Engineering Department, University of Science and Technology, Irbid, Jordan

(*Received* 22 *December* 1994, *and in final form* 5 *February* 1996)

This paper presents the results of investigating the axi-symmetric free vibrations of an isotropic thin oblate spheroidal shell. An oblate spheroid is considered as a continuous system constructed from two spherical shell caps by matching the continuous boundary conditions. This approximation technique is used to express the results in a continuous function analytical formation. The radii and opening angles of the spherical elements are chosen according to the eccentricity of the oblate spheroid.

It is shown that for an ecccentricity: smaller than 0·6 the Rayleigh method reasonably estimates natural frequencies; larger than 0·95 both of the shallow and non-shallow spherical shell theories predict natural frequencies in close agreement; and equal to zero an exact thin sphere solution emerges.

The method presented herein is clearly an engineering approximation for special purpose shells and does not require the computer storage of numerical methods. Also, it may be quite useful when utilised judiciously in many applications, such as in force response analysis. Comparison is made between the present technique, the Rayleigh method, and experimental data for two laboratory models. The formulation can be extended to many types of oblate spheroids with different support conditions and still retain the functional representation.

1. INTRODUCTION

Oblate spheroidal shells have many practical applications; two of these are liquid oxygen tanks used in several upper stages of space vehicles and the protective shell used as the housing of the early-warning scanner of airborne warning and control system aircraft (AWACS). Analytical solutions for such shells are inadequately investigated due to the complexity of the governing equations and the difficulty of obtaining their solutions.

While the literature on free and forced vibrations of spherical shells is almost endless [1–3], only a few papers deal with the free vibrations of oblate thin speroids. Penzes and Burgin [4] solved the problem of free vibrations of a thin isotropic oblate spheroidal shell by Galerkin's method. Membrane theory and harmonic, axisymmetric motion were assumed to derive the differential equations of motion. It was shown that Galerkin's method yields the exact solution for a closed spherical shell as the eccentricity of the oblate spheroid approaches zero. This work was extended by Penzes [5] to include orthotropic oblate spheroids. On the other hand, Combou [6] aimed at studying the axisymmetric vibrations of prolate spheroidal shells with small eccentricities. However, it was stated that for applying his solution to an oblate spheroidal shell, the sign of one of the parameters used in the analysis must be changed.

† Present address: Auckland Institute of Technology, Private Bag 92006, Auckland 1020, New Zealand.

0022–460X/97/290561 + 14 $25.00/0/sv960898

In the present paper the free vibration characteristics of an oblate spheroidal shell are investigated by considering an approximate practical model for the thin oblate spheroid. This model consists of two identical thin spherical shells (caps) closed at the apex and rigidly joined together at their edges. The radius and opening angle of the caps are governed by the major and minor axes of the oblate spheroid. Explicit solutions using non-shallow and shallow shell theories [7, 8] are used for the caps and the frequency equation is deduced by using the continuity of the boundary conditions. Although the proposed model is not general from the theoretical point of view, nevertheless, it is quite useful for many oblate shells of practical applications. To check the practicality of this approximation, and because of the lack of numerical data in the literature, the Rayleigh method is used to predict upper bound frequencies, and the natural frequencies and modes of two experimental models are investigated.

2. PROBLEM FORMULATION

The problem of vibrations of a thin oblate spheroidal shell of thickness h, radii of curvature R_θ and R_ϕ, and principle semi-axes a and b along the major and minor axes, respectively, may be treated by considering the spheroid as a structure composed of two spherical caps rigidly joined at their ends. These caps have, mass density ρ, Young's modules of elasticity E, Poisson ratio v, and their centres of curvature fall along the minor axis of the proposed structure as shown in Fig 1. Such an approximation is not far from reality, as oblate spheroidal tanks are normally produced by joining, either by welding or riveting, two spherical caps through a toroidal shell. The effective radius R_r of the oblate spheroidal model represents the radius of curvature at the cap apex. This can be obtained from the geometrical relation, (see Fig 1),

$$R_\phi = \frac{a(1-e^2)}{(1-e^2\cos^2\phi')^{3/2}}, \tag{1}$$

where ϕ' is the oblate spheroid angle. Setting ϕ' to zero gives

$$R_r = a/(1-e^2)^{1/2}, \tag{2}$$

where e is the eccentricity ratio defined by $e = \sqrt{1-(b/a)^2}$. However, an approximate opening angle for the model ϕ_0 may be obtained by using the following formula:

$$\phi_0 = \cos^{-1}[(R_r - b)/R_r]. \tag{3}$$

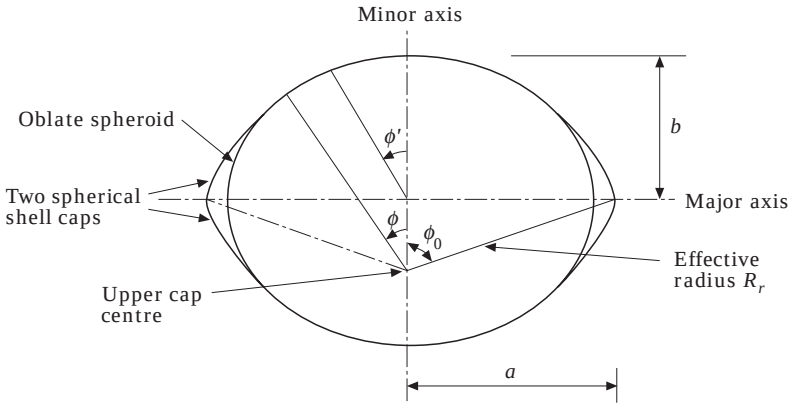

Figure 1. An oblate spheroidal shell approximated by two spherical caps.

Figure 1, which resembles the approximate oblate shell, indicates that the geometry of the oblate and the proposed model are almost the same in the region where the two surfaces coalesce; however, divergence exists close to the boundaries. Further, Fig 2 shows the effective radius and opening angle of the proposed model versus the eccentricity of the oblate spheroid, which indicates that closer geometrical approximation is expected between the exact and approximate model at values of e smaller than 0·6.

3. NON-SHALLOW SHELL THEORY

The equations of motion, which include the bending effect for a spherical shell, are well developed in the literature [9]. Assuming that the temporal and spatial-dependence of free vibrations are separable, the transverse displacement w and the tangential displacement u may be assumed to be

$$w(\phi, t) = W(\phi)\cos\omega t, \qquad u_\phi(\phi, t) = U_\phi(\phi)\cos\omega t, \tag{4}$$

where ω is the circular frequency, t is time and ϕ denotes the angle measured from the vertical axis. The ϕ-dependent variables are given by

$$W(\phi) = \sum_{j=1}^{3} (A_j \mathrm{P}_{nj}(x) + B_j \mathrm{Q}_{nj}(x)), \quad U_\phi(\phi) = \sum_{j=1}^{3} (1+\upsilon) D_j [A_j \mathrm{P}'_{nj}(x) + B_j Q'_{nj}(x)], \tag{5}$$

where A's and B's are arbitrary constants. The symbols $P_n(x)$ and $Q_n(x)$ denote the Legendre functions of the first and second kind, respectively, a prime denotes derivatives with respect to ϕ, and $x = \cos\phi$. Other parameters are defined as follows:

$$D_j = \frac{1 + (\lambda_j - 2)/[(1+\nu)(1+\xi)]}{1 - \nu - \lambda_j + \xi(1-\nu^2)\Omega^2/(1+\xi)}, \qquad n_j = -0{\cdot}5 + \sqrt{0{\cdot}25 + \lambda_j}, \qquad \xi = 12R_r^2/h^2. \tag{6}$$

The parameters λ_j's are the roots of the cubic equation

$$\lambda^3 - [4 + (1-\nu^2)\Omega^2]\lambda^2 + [4 + (1-\nu)(1-\nu^2)\Omega^2 + (1+\xi)(1-\nu^2)(1-\Omega^2)\lambda + (1-\nu)(1-\nu^2)[\Omega^2 - 2/(1-\nu)][1 + (1+\nu)(\Omega^2 - 1/(1+\nu))] = 0. \tag{7}$$

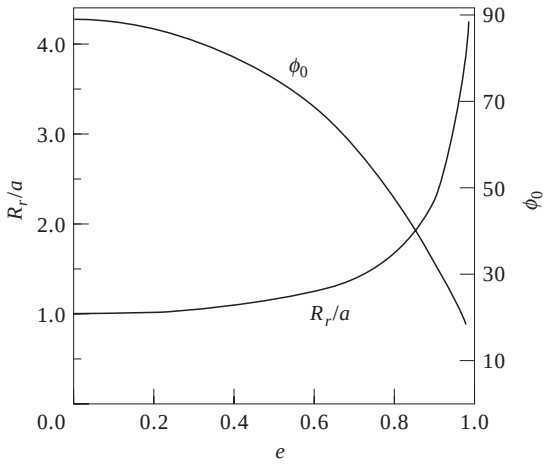

Figure 2. The effective radius/major axis-ratio and opening angle versus eccentricity for the oblate model.

The non-dimensional frequency is defined by

$$\Omega^2 = \rho\omega^2 R_r^2/E \tag{8}$$

The general features of the solutions given by equations (5) depend on the character of the three indices n_1, n_2 and n_3 given by equation (6). The various combinations of complex and real values that the indices may assume are summarised in three zones as follows [7]

Zone I	Zone II	Zone III
$n_1 = b_1$	$n_1 = b_1$	$n_1 = b_1$
$n_2 = b_2 + \mathrm{i}b_3$	$n_2 = -0{\cdot}5 + \mathrm{i}b_2$	$n_2 = b_2$
$n_3 = b_2 - \mathrm{i}b_3$	$n_3 = -0{\cdot}5 + \mathrm{i}b_3$	$n_3 = -0{\cdot}5 + \mathrm{i}b_3$

Here b_1, b_2 and b_3 are real numbers, and $\mathrm{i} = \sqrt{-1}$.

For Zones II and III the Legendre functions of index $-0{\cdot}5 + \mathrm{i}b$ are real quantities and the corresponding values of λ_2 and λ_3 are also real; thus the solution given in the form of equation (5) is directly applicable. However, for Zone I a pair of the Legendre functions have complex conjugate indices and since the deflections W and U_ϕ are real quantities, which implies that the right side of equation (5) must be real too, the solution expressed in terms of real functions may be written as follows:

$$W = \sum C\mathrm{P}_{b1}(x) + C_2\mathrm{Re}[\mathrm{P}_{b2+\mathrm{i}b3}(x)] + C_3\mathrm{Im}[\mathrm{P}_{b2+\mathrm{i}b3}(x)], \tag{9}$$

with $C_2 = A_2 + A_3$ and $C_3 = \mathrm{i}(A_2 - A_3)$.

The two spherical caps are considered to be closed at the apex, $\phi = 0$, and as the Legendre function of the second kind is singular at this point, the constants B in equation (5) are set to zero. The remaining arbitrary constants A or C (three constants for each element) are determined from the boundary conditions. The two caps are assumed rigidly connected along the edge $\phi_1 = \phi_2 = \phi_0$. To insure the continuity of deflections, slopes, moments and forces along the spatial circular junction and taking the top element as reference, the boundary conditions my be written as (See Fig. 3)

$$W_1 - U_{\phi 2}\sin 2\phi_0 + W\cos 2\phi_0 = 0, \qquad U_{\phi 1} - U_{\phi 2}\cos 2\phi_0 - W_2\sin 2\phi_0 = 0,$$
$$\mathrm{d}W_1/\mathrm{d}\phi_1 + \mathrm{d}W_2/\mathrm{d}\phi_2 = 0, \qquad Q_1 - Q_2\cos 2\phi_0 - N_{\phi 2}\sin 2\phi_0 = 0,$$
$$N_{\phi 1} - Q_2\sin 2\phi_0 + N_{\phi 2}\cos 2\phi_0 = 0, \qquad M_1 - M_2 = 0, \tag{10}$$

where subscripts 1 and 2 refer to the upper and lower cap, respectively. Expressions for the membrane stress resultant N_ϕ, the moment resultant M, and the transverse shear forces Q in terms of the displacements $W(\phi)$ and $U_\phi(\phi)$ are determined from reference [7] and used in the above equations. This results in six simultaneous homogeneous equations which are used to determine the eigenvalues and eigenvectors of the posed problem.

4. SHALLOW SHELL THEORY

The applicability of the present approximate model is further investigated by using the shallow shell theory. As the eccentricity of an oblate spheroidal shell approaches values greater than 0·93, the opening angle ϕ_0 of the approximate oblate model reaches the value of 30°. For such an angle the assumptions of shallowness [10] are valid. These assumptions

neglect the contribution of the transverse shearing stress resultants to the equilibrium of forces in the meridian and tangential directions, and neglect the contribution of stretching displacement to the change of curvature expressions. The equations of motion of this theory admit solutions of the form [8]

$$w_r(r, t) = W_r(r) \cos \omega t, \qquad u_r(r, t) = U_r(r) \cos \omega t, \tag{11}$$

where w_r and u_r are the transverse and meridian displacement components, respectively; $W_r(r)$ and $U_r(r)$ take the forms:

$$W_r(r) = \sum_{j=1}^{3} \left\{ A_j \mathrm{J}_0\left(\mu_j \frac{r}{d}\right) + B_j \mathrm{Y}_0\left(\mu_j \frac{r}{d}\right) \right\}$$

$$U_r(r) = 2\frac{H}{d}\left\{ \frac{r}{d} W_r(r) + (1+\nu) \sum_{j=1}^{3} \left[[(1-\nu^2)(h/d)^2(\omega/\omega_0)^2 - \mu_j^2]^{-1} \right.\right.$$

$$\left.\left. \times \left[u_j A_j \mathrm{J}_1\left(\mu_j \frac{r}{d}\right) + \mu_j B_j \mathrm{Y}_1\left(\mu_j \frac{r}{d}\right) \right] \right] \right\}, \tag{12}$$

where A_j and B_j are arbitrary constants; J and Y are the Bessel functions of the first and second kind, respectively; H and d are the shallow shell height and base radius, respectively; and μ_j are the roots of

$$\mu^6 - (1-\nu^2)(h/d)^2(\omega/\omega_0)^2\mu^4 - 12(1-\nu^2)[(\omega/\omega_0)^2 - 4(H/h)^2]\mu^2$$
$$+ 12(1-\nu^2)(h/d)^2(\omega/\omega_0)^2[(1-\nu^2)(\omega/\omega_0)^2 - 8(1+\nu)(H/h)^2] = 0, \tag{13}$$

with $\omega_0 = \sqrt{Eh^2/\rho d^4}$.

For a finite displacement at the apex the constants B are set to zero to avoid the singularity produced by Y_0 and Y_1 at $r = 0$. The remaining six constants A, three for the upper element and three for the lower, are determined from the boundary conditions at $r = d$. Using subscripts 1 and 2 to refer to the upper and lower cap, respectively, these conditions may be written as (see Figure 3(b))

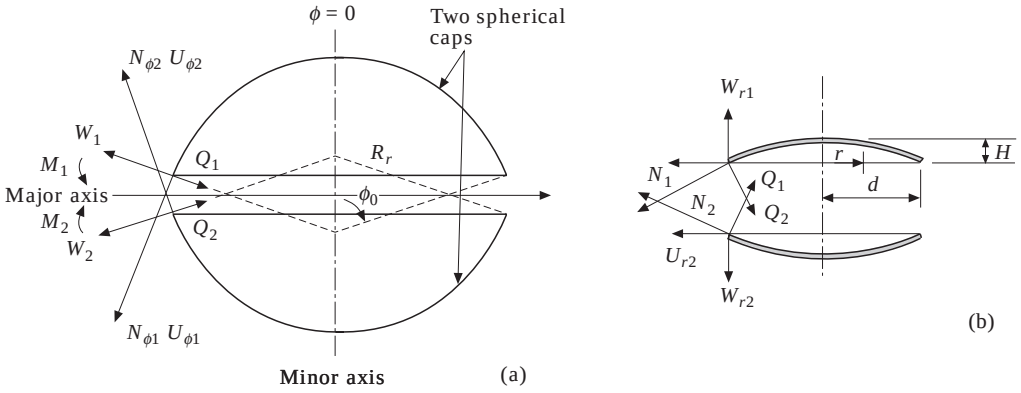

Figure 3. Matching of boundary conditions of two shell-caps: (a) non-shallow shell model; (b) shallow shell model.

$$W_{r1} + W_{r2} = 0, \qquad U_{r1} - U_{r2} = 0, \qquad \left[\frac{\mathrm{d}W_r}{\mathrm{d}r}\right]_1 + \left[\frac{\mathrm{d}W_r}{\mathrm{d}r}\right]_2 = 0,$$

$$N_1 + N_2 \cos 2\phi_0 - Q_2 \sin 2\phi_0 = 0, \quad Q_1 - N_2 \sin 2\phi_o - Q_2 \cos 2\phi_0 = 0, \quad M_1 - M_2 = 0. \tag{14}$$

Expressions for the forces N and Q and the moments M in terms of W_r and U_r are determined [10] and used in equation (14).

Whether using the non-shallow shell theory or the shallow shell theory, the procedure for obtaining the natural frequencies and mode shapes is the same. It consists of substituting the appropriate expressions for W, U, N, M, and Q in the boundary conditions, equations (10) or (14), accordingly, then six simultaneous homogeneous equations in terms of the constants are obtained. These may be written in the form

$$[C_{jk}][A_{jk}] = 0 \qquad (j, k = 1, 2, \ldots, 6) \tag{15}$$

where the coefficients C_{jk} are functions of the natural frequency Ω and are given in the Appendix. The natural frequencies are obtained for given values of ϕ_0, v and h/R by searching for the vanishing determinants $|C_{jk}|$. Once a natural frequency is known, the corresponding mode shape is obtained by evaluating C_{jk} and then determining A_{jk} from equation (15).

5. RAYLEIGH'S ENERGY METHOD

Due to the complexity encountered in solving the exact equations of motion of an oblate spheroidal shell, the Rayleigh method is used to determine the first two natural frequencies of the system under investigation. The Rayleigh quotient for a conservative system may be written as:

$$\omega^2 = U_{max}/K_{max}, \tag{16}$$

with U_{max} and K_{max} as the system maximum potential and kinetic energy, respectively (see Appendix).

If the assumed mode shapes satisfy all boundary conditions, equation (16) results in an upper bound approximation. However, many investigators [11] have established the fact that it is sufficient to satisfy deflection and slope conditions only and achieve acceptable approximations of natural frequency. In solving the equations of kinetic and potential energy of a complete oblate spheroidal shell, it should be noted that there are no physical boundary conditions. However, the only conditions to be imposed are that the displacements should be single-valued and bounded at every point of the shell, including the north and south poles. This fact is in resemblance to that of a thin sphere. Based on this argument, reference [4] shows that for many applications using the thin sphere mode shapes to represent those of an oblate spheroid as an acceptable assumption. Therefore, in the present work the first two mode shapes of a spherical shell are considered to satisfy the boundary conditions of an oblate spheroidal shell and assumed to take the form

$$W = \sum_{j=0}^{n} a_j \phi'^j, \qquad U_\phi = -f \sin 2\phi', \tag{17}$$

where a's and f are related coefficients and the ratios f/a are chosen carefully to represent the approximate modes.

TABLE 1
Specification of tested models

Parameter	Model 1	Model 2
a(m)	0·185	0·18
b(m)	0·135	0·07
e	0·683	0·921
h(mm)	1·5	1·5
E(GPa)	68	68
ρ(kg/m^3)	2720	2720
v	0·3	0·3

A fifth order polynomial is used for W. However, to check its accuracy, the first two natural frequencies and modes of a full thin sphere were determined by using equation (17) as well as by using the exact solution [3] and prove to be in good agreement. The coefficients of this polynomial are given in the Appendix for different values of e. Substitution of the assumed modes in equation (16) and selecting appropriate values for the shell properties results in upper bound values of the first two natural frequencies associated with the first two modes for various values of e.

6. EXPERIMENTAL WORK

Two aluminium spheroidal shell models with the specifications given in Table 1 were constructed. Each model was formed by using two identical shell elements with a half of an ellipse cross-section. These elements were formed by making use of spinning techniques as follows: A profile forming wooden plate was made to be the negative of the required shape of half an ellipse. This plate was used to produce a cast iron pattern of the desired shape. The blank to be formed is forced to follow the iron pattern, which was attached to the chuck of a lathe machine, to assume its shape. The two shell elements were then stuck together using special aluminium filled adhesive paste ensuring the continuity of the two elements to form a closed spheroidal shell. The rigidity of the joined ends were checked by applying different impact loads and proved to be well suited for the purpose of the present experiments.

Theories indicate that the amplitude of radial motion in axisymmetric modes is maximum at the apex. As the aim of the present work is to excite axisymmetric modes only, ensuring at the same time free edges, one of the apexes was joined directly through a bolt and nut to an electromechanical shaker and the response was measured at the other apex in order to exclude any non-symmetrical modes. The shaker was excited through an amplifier at various frequencies and a resonance was distinguished by observing the sharp increase in the amplitude of the piezoelectric transducer output displayed on an oscilloscope, and by the emitted acoustic tone. Once a natural frequency was recorded the exciting frequency held fixed and the transducer slowly and lightly moved along the meridian and tangential directions to trace nodal lines associated with the natural frequency. Mode shapes were then reported after normalisation in Figure 8.

7. RESULTS AND DISCUSSION

The lack of numerical results concerning the undergoing problem, the complexity of obtaining a closed form solution for the free vibration characteristics of an oblate spheroid, and in an attempt to investigate the practicality and feasibility of the present theoretical

TABLE 2
Natural frequencies in Hz *for a full sphere* [3]

m	DAS	BMM	RM
2	5281	5284	5335
3	6321	6323	6510
4	6883	6884	—†

†Not predicted.

model the following steps are taken: (1) The developed model is general and to test its validity the natural frequencies for a thin sphere, which is considered as an ultimate shape of the oblate spheroid, are determined. This is done by setting the eccentricity to zero in the present boundary matching method and the results are compared with the values given by Tavakoli and Singh [3] using the direct analytical solution DAS. Table 2 shows the natural frequencies of the first three axi-symmetric modes of a full sphere of 0·1143 m radius and 5·7 mm thickness with material properties of $E = 207$ GPa, $\rho = 7800$ kg/m^3 and $v = 0{\cdot}3$. These frequencies were obtained by applying the DAS and the two methods adopted in this work, namely, the Rayleigh method RM and the boundary matching method BMM. From Table 2 it can be perceived that the DAS and the BMM methods give natural frequencies within computational errors. This is attributed to the fact that the latter method is nothing but another approach for obtaining closed form solutions. (2) The Rayleigh method is used for the matter of comparison as well as for further investigation. Table 2 obviously shows that the Rayleigh method predicts frequencies higher than the other two methods. This fact is inherent in this method for its higher bound prediction. (3) Table 3 gives the results for the natural frequencies of the two tested models with the specifications given in Table 1. These results are obtained by using the BMM, RM and the experimental investigations for two values of e. The theoretical values predicted by the BMM are, in general, higher than the corresponding experimental values for $e = 0{\cdot}683$ and lower than those for $e = 0{\cdot}921$. This may be attributed to the fact that in the former the theoretical caps are stiffer than the corresponding experimental ones while in the latter the theoretical model approaches a plate ($e = 0{\cdot}921$) which has less stiffness. Therefore, from the above results, it may be concluded that the two methods used in this work give feasible results for moderate values of e and may be used for further study.

One of the main indices of an oblate spheroid is its eccentricity e. Fig. 4 depicts the non-dimensional natural frequency Ω of the first two modes of vibration as a function of e, obtained by using the RM and the BMM based on the non-shallow shell theory. It is shown that the natural frequency decreases as e increases. Also it is indicated that the curve obtained by the RM adjoins to that of the BMM with slightly higher values until e reaches 0·6 where the former starts to diverge. This behaviour could be explained by the fact that

TABLE 3
Natural frequencies in Hz for the tested models

	$e = 0{\cdot}683$			$e = 0{\cdot}921$		
Frequency	BMM	RM	Experimental	BMM	RM	Experimental
1	2500	3100	2400	1574	4246	1557
2	2978	3398	2600	1734	3248	1950
3	3082	–	2900	1744	–	2100

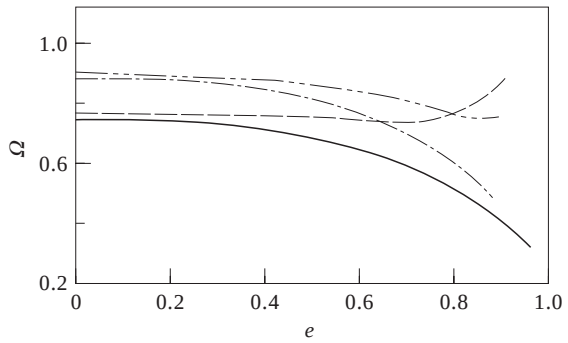

Figure 4. Non-dimensional natural frequency versus eccentricity ratio: ——, first mode BMM; — —, first mode RM, – · –, second mode BMM; — · · —, second mode RM.

the mode shapes of a closed thin sphere, employed by RM, would resemble those of an oblate spheroid up to certain eccentricity. As e increases the oblate spheroid tends to flatten up. Such "flattening" causes the uncoupling of the transverse motion and the tangential motion, where the latter is minimised and the former approaches that of a circular plate (a circular plate is an oblate one with $e = 1$). However, large divergence is exhibited by the RM for e greater than 0·6. This is attributed to the additional constraints of deviation from a true mode shape which causes larger values of potential energy and thus the natural frequency abruptly diverges to higher values with larger e. Therefore, values of Ω predicted by the RM are in tremendous error for e larger than 0·6. This fact is clearly emphasised in the values given in Table 3 where the RM gives large error for $e = 0{\cdot}921$.

In this work eg. an oblate spheroid of $e = 0{\cdot}93$ and larger might be modelled as a structure composed of two shallow spherical shell caps rigidly joined together at their edges with an opening angle 30° or less as shown in Fig 3. Figure 5 shows that both of the non-shallow and shallow shell theories predict natural frequencies with acceptable convergence. Further the two theories predict very close frequencies for $e \geqslant 0{\cdot}98$. However, for $e < 0{\cdot}93$, the opening angle of the approximate spherical shell model exceeds 30° and thus the assumptions of shallowness will no longer hold.

To further examine the validity of the proposed model, as well as to investigate the effect of the thickness ratio h/a, the first ten bending modes and the first two membrane modes for an oblate shell with $e = 0$ were reproduced and the results match that given by Fig. 2

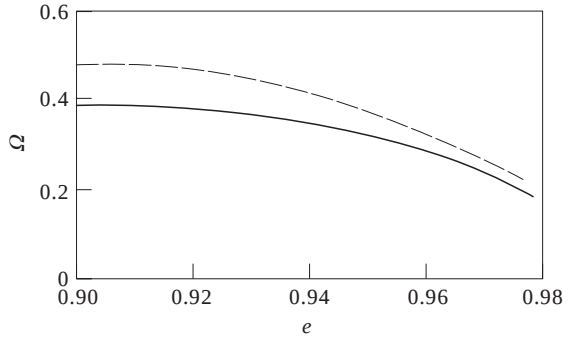

Figure 5. Non-dimensional natural frequency versus eccentricity ratio: ——, non-shallow theory; — —, shallow theory.

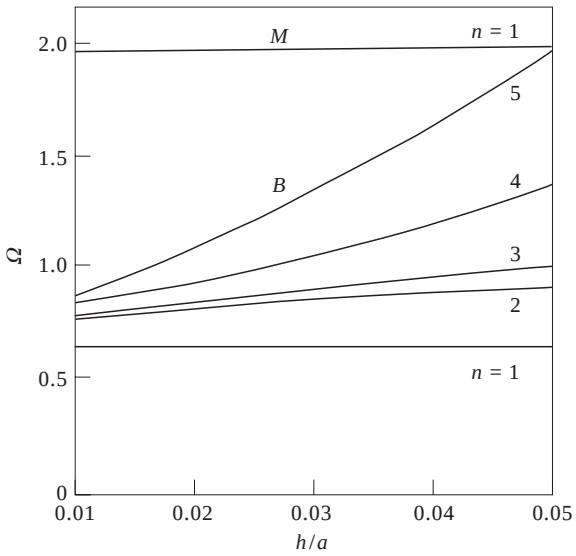

Figure 6. Non-dimensional natural frequency versus h/a of an oblate model with $e = 0{\cdot}6$ using BMM.

of Kalnins [7] (is is not given here for brevity), with negligible computational errors. However, using the non-shallow shell theory, Fig. 6 shows the first few frequencies as functions of the thickness ratio for $e = 0{\cdot}6$ and $v = 0{\cdot}3$. It is shown that the natural frequencies of the bending modes increase with the thickness ratio. Since the membrane modes occur at relatively high values of Ω in comparison to the bending modes, only the first of the former modes is considered. A conclusion is reached, which is identical to that of a full sphere [7], is that the membrane modes have very small variation with the thickness ratio.

Figure 7 shows the variation of the natural frequency of the first three bending modes and the first membrane mode as a function of e. It is clearly observed that as e increases, the natural frequencies associated with the bending modes decrease and that associated with the membrane mode increases. Steeper variations are observed for $e \geqslant 0{\cdot}5$ where the

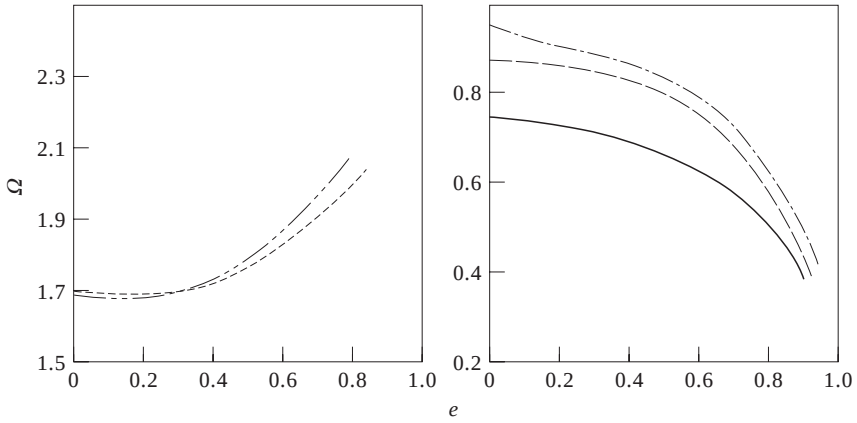

Figure 7. Non-dimensional natural frequency versus e for different modes: ——, first bending mode; — —, second bending mode; — · —, third bending mode; – · · –, membrane mode BMM; - - - -, membrane mode RM.

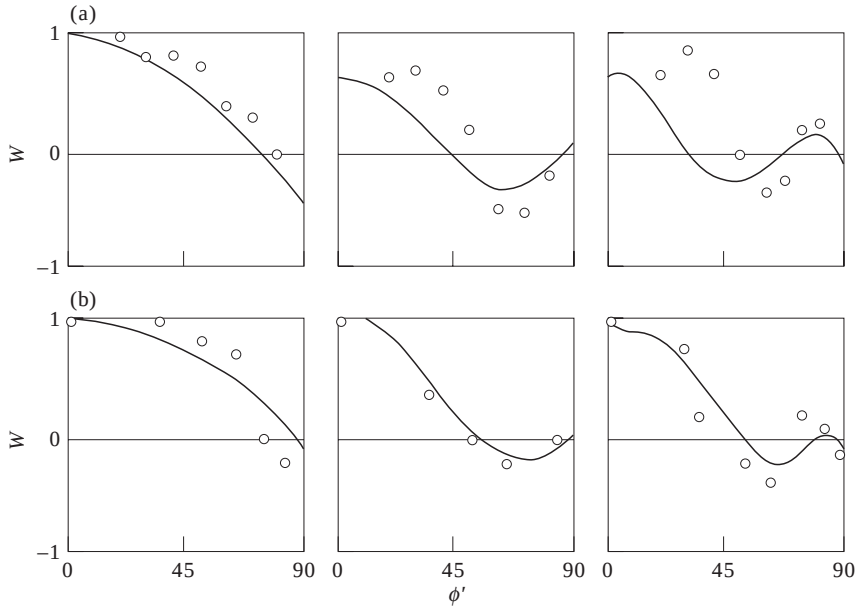

Figure 8. Normalized mode shapes associated with the first three natural frequencies of Table 3: ——, theoretical based on non-shallow theory; . . . , experimental. (a) $e = 0{\cdot}683$; (b) $e = 0{\cdot}921$.

bending frequency curves converge to very close values. Similar behaviour was observed [12] for a cylindrical shell with an elliptical cross-section. This behaviour is attributed to the geometrical structure of the shell. As e increased from zero, the shape of the oblate spheroid departs from being a full sphere toward being a flat plate which has a stiffness lower than that of a sphere. Thus the first axisymmetric natural frequency increases by introducing a slight curvature to a circular plate. On the other hand the membrane mode shows an opposite behaviour which is attributed to the fact that the stretching strain energy for a flat plate is dominant and thus the natural frequency becomes larger with e. Both of the BMM and the RM are used to show the latter behaviour.

The modes of vibration can be easily determined from equation (15). Using the non-shallow shell theory, Fig. 8 shows the modes of vibration for the two experimental models. The experimental modes are obtained after normalisation with respect to the apex. Exploring these modes indicates that the experimental and theoretical modes have the same trends of variation and they have the same nodal lines.

8. CONCLUSIONS

Although it is customary to use methods such as finite elements to handle the vibration characteristics of an oblate shell, the present approximation, in general, seems not to have been done before. The present model is of course only approximate, but the results are reassuring for many practical shells. Further, this approximation model is handy and may be utilised where closed formulation is needed such as in using modal analysis for forced response. This can easily be done by using Fig. 2 to obtain the approximate effective radius R_r and angle ϕ_0. The model predicts reasonably well the free vibration natural frequencies and mode shapes for different values of eccentricity ratio. However, the Rayleigh method is of no use for eccentricities less than 0·6.

REFERENCES

1. A. W. Leissa 1973 *Vibration of Shells* NASA SP-288, U.S. Government Printing Office, Washington D.C.
2. V. C. M. De Souza and J. G. A. Croll 1983 *Journal of Strain Analysis* **18**, 27–36. Vibration tests on spherical shell caps.
3. M. S. Tavakoli and R. Singh 1989 *Journal of Sound and Vibration* **100**, 97–123. Eigensolutions of joined/hermetic shell structures using the state space method.
4. L. E. Penzes and G. H. Burgin 1965 *General Dynamics Report* No. **GD/C-BTD**, 65–113. Free vibrations of thin isotropic oblate spheroidal shells.
5. L. E. Penzes 1969 *Journal of The Acoustical Society of America* **45**, 500–505. Free vibrations of thin orthortropic oblate spheroidal shells.
6. J. P. Cambou 1975 *Acustica* **34**, 72–76. Vibrations libre et axisymetrique des reservoirs quasi-spherique.
7. A. Kalnins 1964 *Journal of the Acoustical Society of America* **36**, 74–811. Effect of bending on vibrations of spherical shells.
8. A. Kalnins 1963 *Proceedings of the fourth U.S. National Congress of applied Mechanics, University of California, Berkeley*, 225–233. Free nonsymmetric vibrations of shallow spherical shells.
9. P. M. Naghdi and A. Kalnins 1962 *Journal of Applied Mechanics* **29**, 65–72. On vibrations of elastic spherical shells.
10. E. Reissner 1953 *Journal of Mathematical Physics* **38**, 16–35. On the determination of stresses and displacements for unsymmetrical deformations of shallow spherical shells.
11. W. Soedel 1981 *Vibrations of Shells and Plates*. New York. Marcel Dekker, Inc.
12. J. L. Sewall and C. G. Pusey 1971 *American Institute of Aeronautics and Astronautics Journal* **9**, 1004–1011. Vibration study of clamped-free elliptical cylindrical shells.

APPENDIX

A.1. THE COEFFICIENTS C_{jk}

The coefficients of equation (15) are summarised below:

A.1.*a*. *Non-shallow shell case*

$$C_{1k} = \mathrm{P}_{nk}(\cos\phi_0), \qquad C_{2k} = -(1+\nu)D_k\mathrm{P}'_{nk}(\cos\phi_0), \qquad C_{3k} = \mathrm{P}_{nk}(\cos\phi_0),$$

$$C_{4k} = \frac{h^3}{12(1-\nu^2)R_r^3}\,[1+(1+\nu)D_k)(\nu+\lambda_k-1)\mathrm{P}_{nk}(\cos\phi_0)]$$

$$C_{5k} = \frac{h}{(1-\nu^2)R_r}\,[(1+D_k\lambda_k)\mathrm{P}_{nk}(\cos\phi_0) + (1-\nu)\cot\phi_0 D_k\mathrm{P}'_{nk}(\cos\phi_0)]$$

$$C_{6k} = \frac{h}{12(1-\nu^2)R_r^2}\,(1+(1+\nu)D_k)[\lambda_k\nu\mathrm{P}_{nk}(\cos\phi_0) - (1-\nu)\cot\phi_0\mathrm{P}'_{nk}(\cos\phi_0)], \tag{A1}$$

with $k = 1, 2, 3$. However, for $k = 4, 5, 6$ the coefficients are

$$C_{1j} = -C_{2j}\sin 2\phi_0 + C_{1j}\cos 2\phi_0, \quad C_{2k} = -C_{2j}\cos 2\phi_0 - C_{1j}\sin\phi_0, \quad C_{3k} = C_{3j},$$

$$C_{4k} = -C_{4j}\cos\phi_0 - C_{5j}\sin 2\phi_0, \quad C_{5k} = C_{4j}\sin 2\phi_0 - C_{5j}\cos 2\phi_0, \quad C_{6k} = -C_{6j}, \tag{A2}$$

where $j = k - 3$.

A.b. Shallow shell case

$$C_{1k} = \mathrm{J}_0(\mu_k) + \frac{(1+\nu)\mu_k \mathrm{J}_1(\mu_k)}{(1-\nu^2)(h/d)^2(\omega/\omega_0)^2 - \mu_k^2},$$

$$C_{2k} = \mathrm{J}_0(\mu_k), \qquad C_{3k} = \mu_k \mathrm{J}_1(\mu_k),$$

$$C_{4k} = \frac{h}{R_r}\left[\frac{\mu_k \mathrm{J}_1(\mu_k) + (1+\nu)(h/d)^2(\omega/\omega_0)^2 \mathrm{J}_0(\mu_k)}{(1-\nu^2)(h/d)^2(\omega/\omega_0)^2 - \mu_k^2}\right],$$

$$C_{5k} = -\frac{h^3}{12(1-\nu^2)d^3}[\mu_k^3 \mathrm{J}_1(\mu_k)],$$

$$C_{6k} = -\frac{h^3}{12(1-\nu^2)d^2}[\mu_k(1-\nu)\mathrm{J}_1(\mu_k) - \mu_k \mathrm{J}_0(\mu_k)], \tag{A3}$$

with $k = 1, 2, 3$. However, for $k = 4, 5, 6$ the coefficients are

$$C_{1k} = -C_{1j}, \qquad C_{2k} = C_{2j}, \qquad C_{3k} = C_{3j},$$

$$C_{4k} = C_{4j}\cos 2\phi_0 - C_{5j}\sin 2\phi_0, \quad C_{5k} = -C_{4j}\sin 2\phi_0 - C_{5j}\cos 2\phi_0, \quad C_{6k} = -C_{6j}, \tag{A4}$$

where $j = k - 3$.

A.2. ENERGY METHOD

An expression for the maximum potential energy was derived and may be written as

$$U_{\max} = \frac{Eh}{2R_\phi^2(1-\nu)^2}\int_0^{2\pi}\int_0^{2\pi}\left\{\frac{h^2}{12R_\phi}\left[\left[\frac{\mathrm{d}}{\mathrm{d}\phi'}\left(U_\phi - \frac{\mathrm{d}W}{\mathrm{d}\phi'}\right)\right]^2 + \frac{\tan^2\phi'}{R_\theta^2}\left[U_\phi - \frac{\mathrm{d}W}{\mathrm{d}\phi'}\right]^2\right.\right.$$

$$+\frac{2\nu\tan\phi'}{R_\theta R_\phi}\left[U_\phi - \frac{\mathrm{d}W}{\mathrm{d}\phi'}\right]\frac{\mathrm{d}}{\mathrm{d}\phi'}\left(U_\phi - \frac{\mathrm{d}W}{\mathrm{d}\phi'}\right)\Bigg] + \left[\frac{\mathrm{d}U_\phi}{\mathrm{d}\phi'} + W\right]^2$$

$$+\frac{R_\phi^2}{(R_\theta\sin\phi')^2}(U_\phi\cos\phi' + W\sin\phi')^2 + \frac{2R_\phi\nu}{R_\theta\sin\phi'}\left[\frac{\mathrm{d}U_\phi}{\mathrm{d}\phi'} + W\right]$$

$$\left.\times(U_\phi\cos\phi' + W\sin\phi')\right\}R_\phi R_\theta\sin\phi'\,\mathrm{d}\phi'\,\mathrm{d}\theta. \tag{A5}$$

TABLE 4
Power series coefficients

e	ϕ_o	R_r	a_0	a_1	a_2	a_3	a_4	a_5	b
0·0	90	20	1·0	0·0163	−1·598	0·137	0·517	−0·123	0·5
0·3	85	21	1·0	0·0163	−1·599	0·137	0·517	−0·123	0·5
0·6	70	24	1·0	−0·0504	−2·231	2·021	−2·094	1·024	0·37
0·8	53	30	1·0	0·2090	−3·300	3·0	−4·2	3·040	0·35
0·95	27	57	0·916	−0·144	−5·563	−17·6	63·4	−37·27	0·15

The maximum kinetic energy expression is

$$K_{\max} = \frac{\omega^2 \rho h}{2} \int_0^{2\pi} \int_0^{2\pi} (U_\phi^2 + W^2) R_\phi R_\theta \sin \phi' \, \mathrm{d}\theta \, \mathrm{d}\phi', \tag{A6}$$

where $R_\theta = a/(1 - e^2 \cos^2 \phi')^{1/2}$

Equating the maximum kinetic energy to the maximum potential energy, an expression for the natural frequency is obtained.

The constants in equation (17) were carefully selected to match the first and second modes [7] for different values of e and are given in Table 4. The values of R_r and ϕ_0 are determined from equation 2 and 3, respectively.